Supporting Information

Coordination structure of the Fe-585DV/N_xC_{4-x} on the electrocatalytic performance of Oxygen Reduction Reactions

Ren Li, [†a] Lei Zhang, [†b] Yi Wang, [a] Jinbo Bai, [c] Xiaolin Li, [d*] and Chunmei Zhang [e*]

Generation of OH*O* and OH*OH* pathways in the ORR (Oxygen Reduction Reaction) process:

$$O_2^* + 2H_2O + 4e^- \rightarrow OH^*O^* + OH^- + H_2O + 3e^- \#(1)$$

$$OH^*O^* + OH^- + H_2O + 3e^- \rightarrow OH^*OH^* + 2OH^- + 2e^- \#(2)$$

$$OH^*OH^* + 2OH^- + 2e^- \rightarrow OH^* + 3OH^- + e^- \#(3)$$

$$3OH^- + OH^* + e^- \rightarrow 4OH^- \#(4)$$

Where * stands for an active site on the catalyst. The intermediates of the ORR reaction, including OO*, OH*O*, OH*OH*, and OH*, are adsorbed onto the active sites.

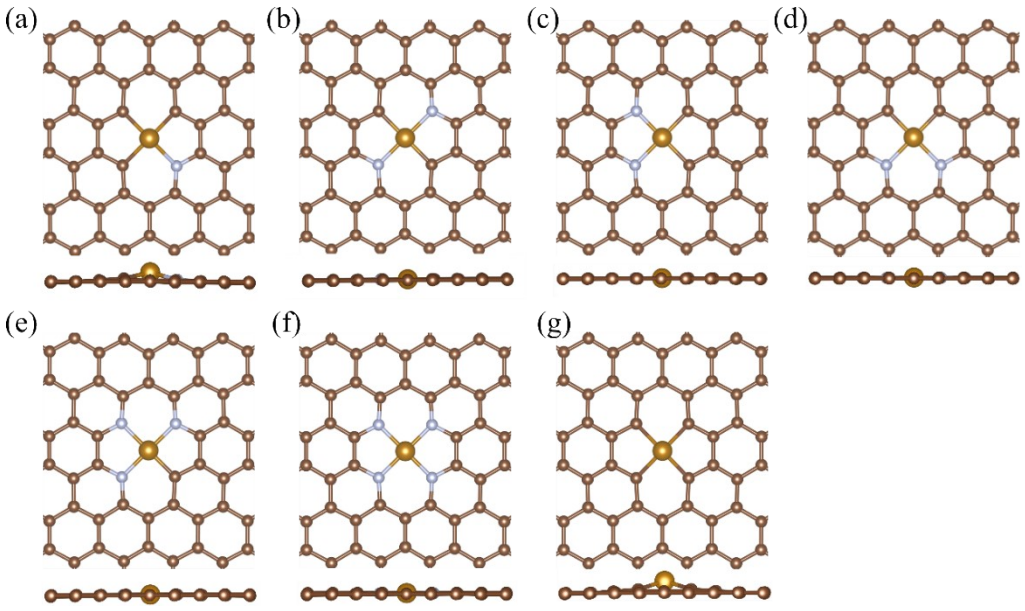

Figure S1. The geometry optimization structures of a. Fe-N_1C_3, b. Fe-N_2C_2(I), c. Fe-N_2C_2(II), d. Fe-N_2C_2(III), e. Fe-N_3C_1, f. Fe-N_4, g. Fe-C_4. The large yellow, small brown, and gray balls represent Fe, C and N atoms, respectively.

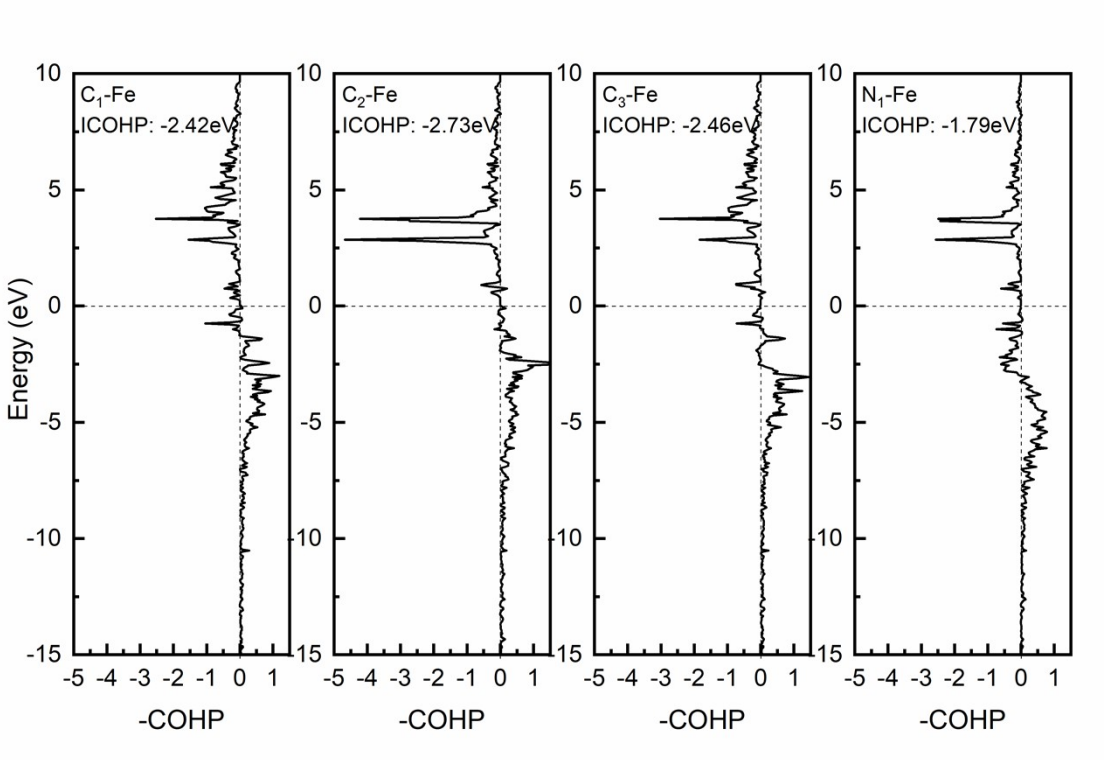

Figure S2(a). Fe-N_1C_3 coordination structure with Fe-C and Fe-N bond COHP.

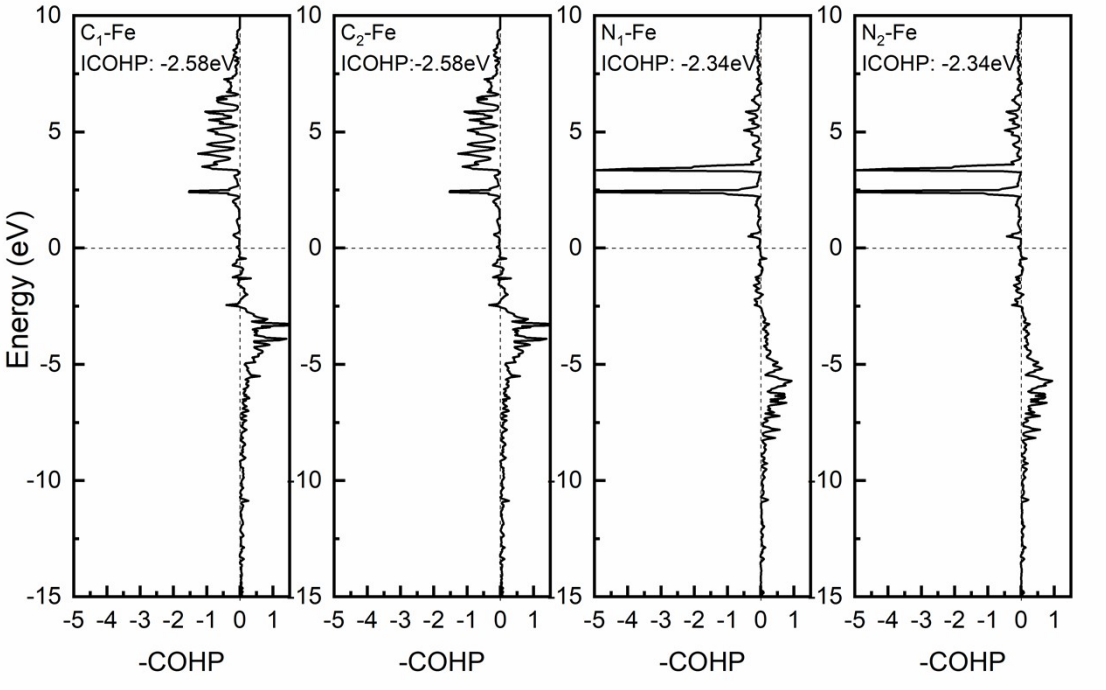

Figure S2(b). Fe-N_2C_2(I) coordination structure with Fe-C and Fe-N bond COHP.

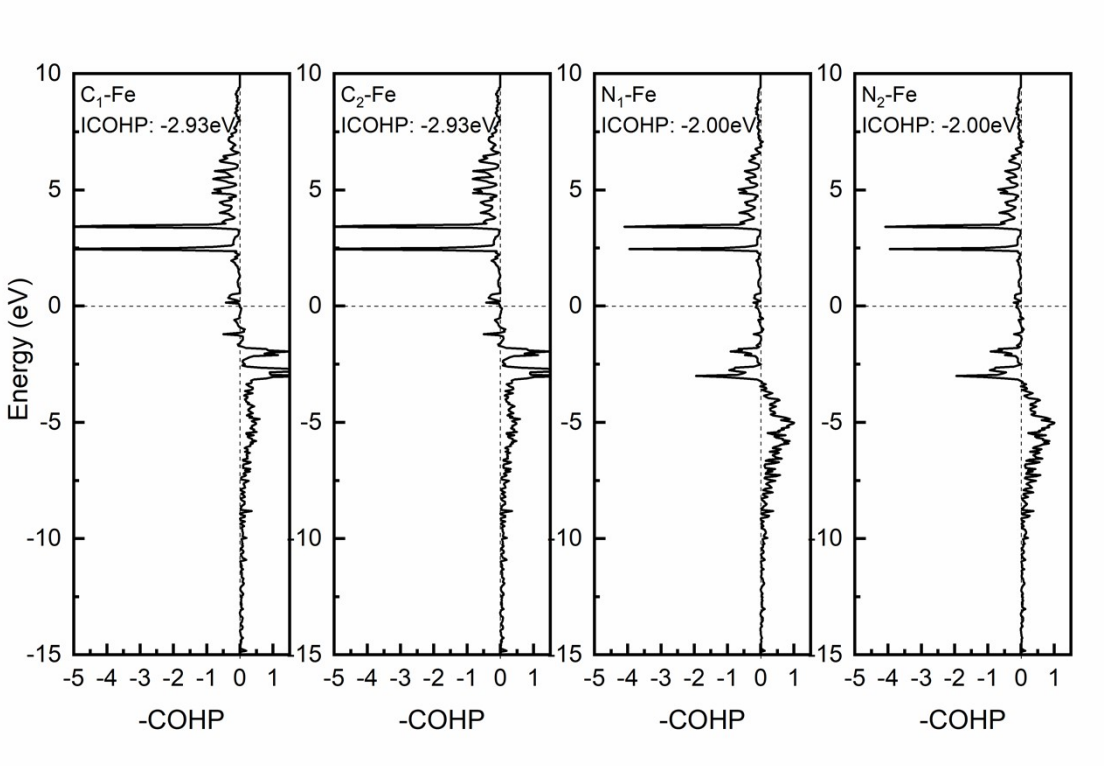

Figure S2(c). Fe-N_2C_2(II) coordination structure with Fe-C and Fe-N bond COHP.

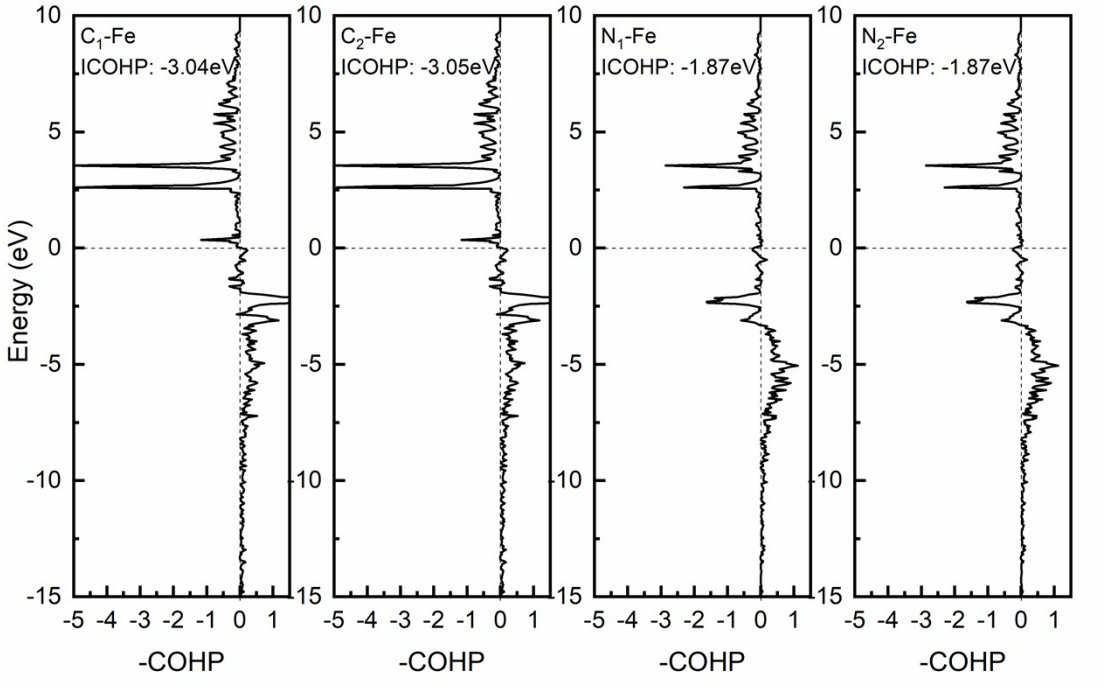

Figure S2(d). Fe-N_2C_2(III) coordination structure with Fe-C and Fe-N bond COHP.

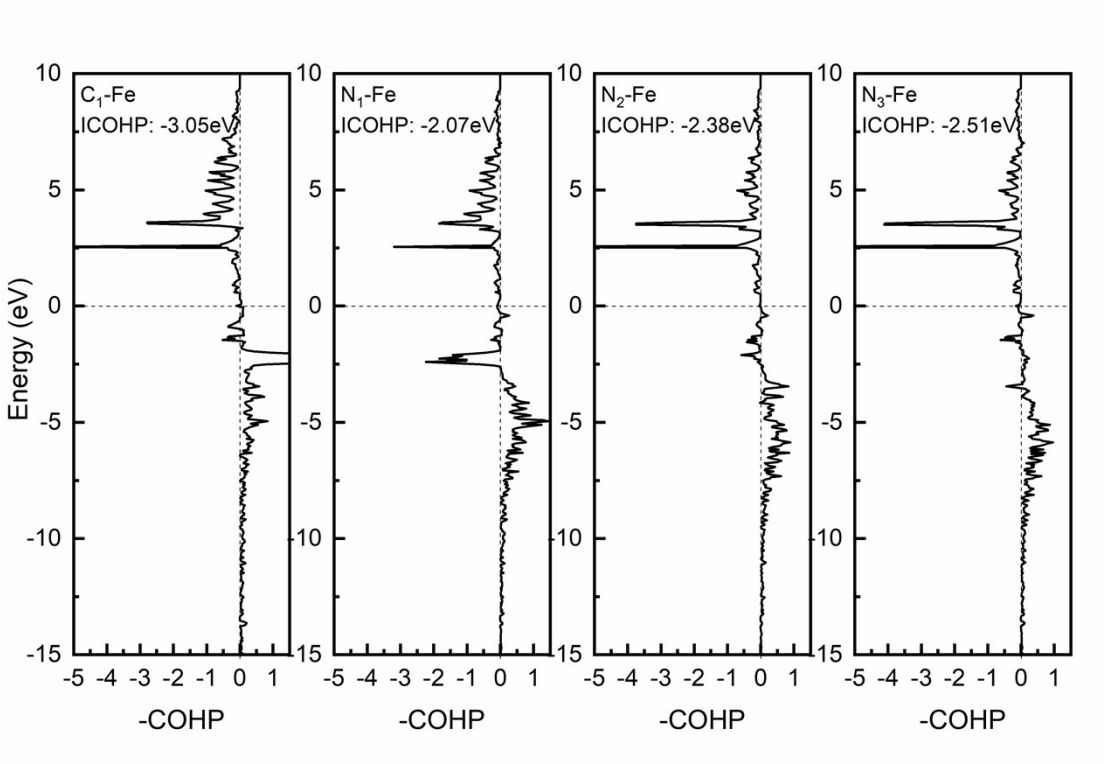

Figure S2(e). Fe-N_3C_1 coordination structure with Fe-C and Fe-N bond COHP.

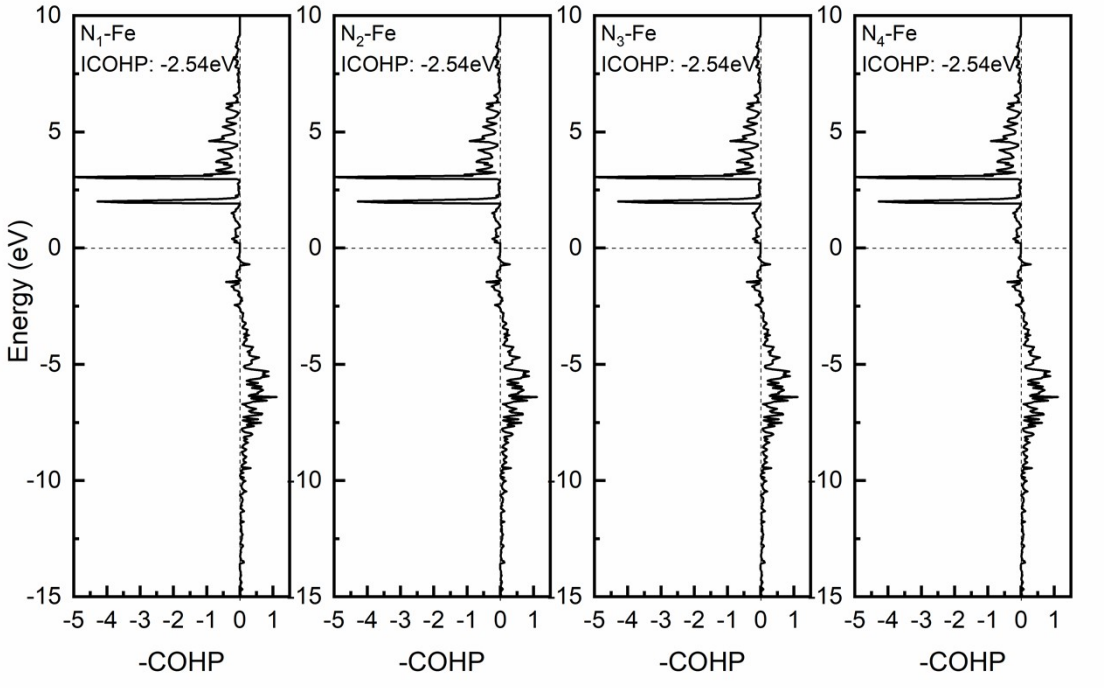

Figure S2(f). Fe-N_4 coordination structure with Fe-N bond COHP

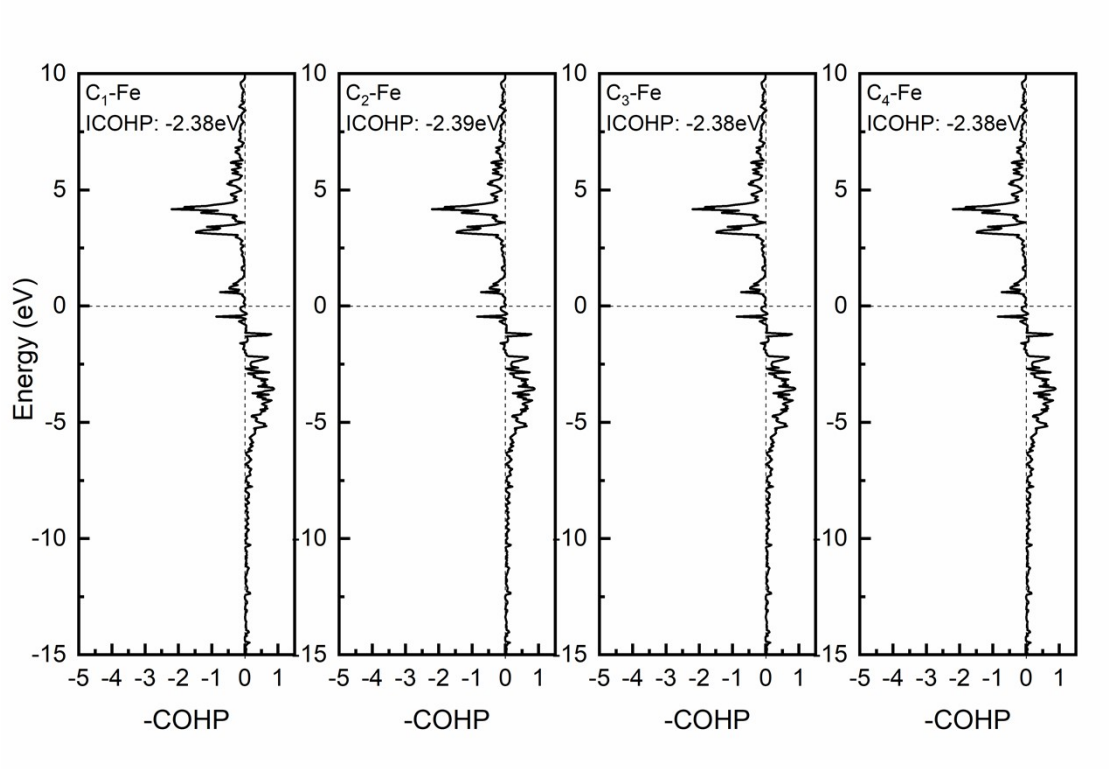

Figure S2(g). Fe-C_4 coordination structure with Fe-C bond COHP.

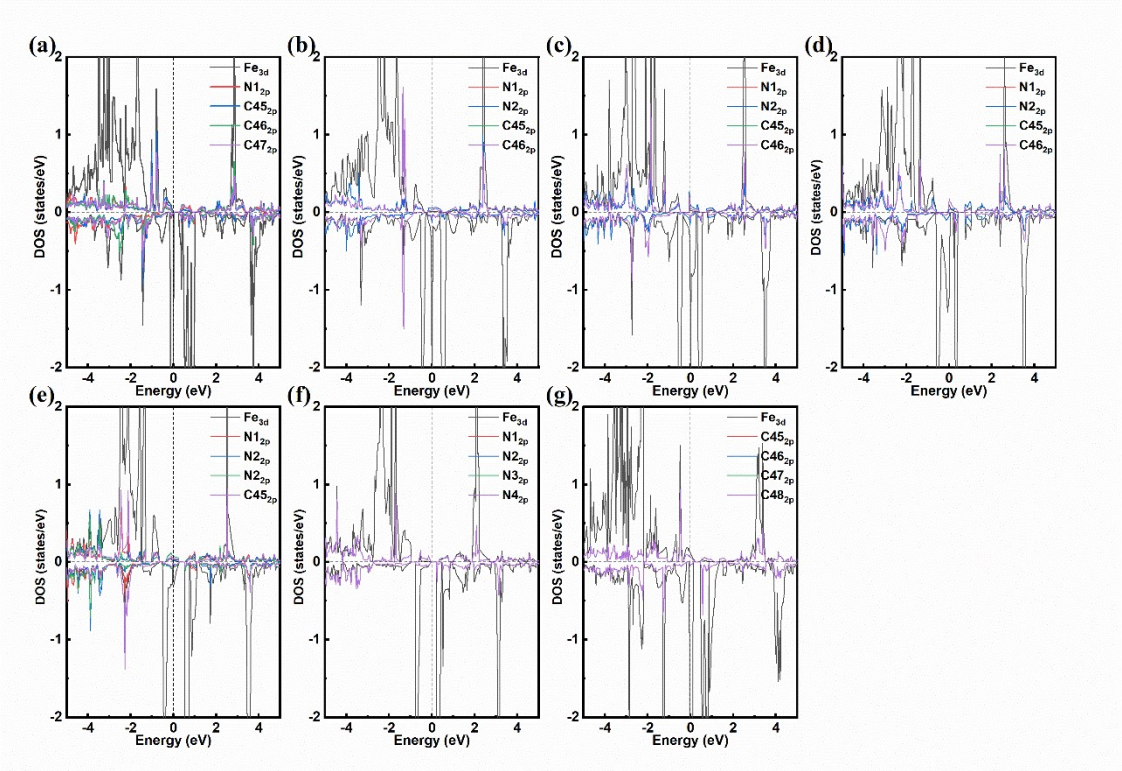

Figure S3. Fe and neighboring N and C projected state density for different Fe-585DV/$N_xC_{(4-x)}$ structures. (a). Fe-N_1C_3, (b). Fe-N_2C_2(I), (c). Fe-N_2C_2(II), (d). Fe-N_2C_2(III), (e). Fe-N_3C_1, (f). Fe-N_4, (g). Fe-C_4.

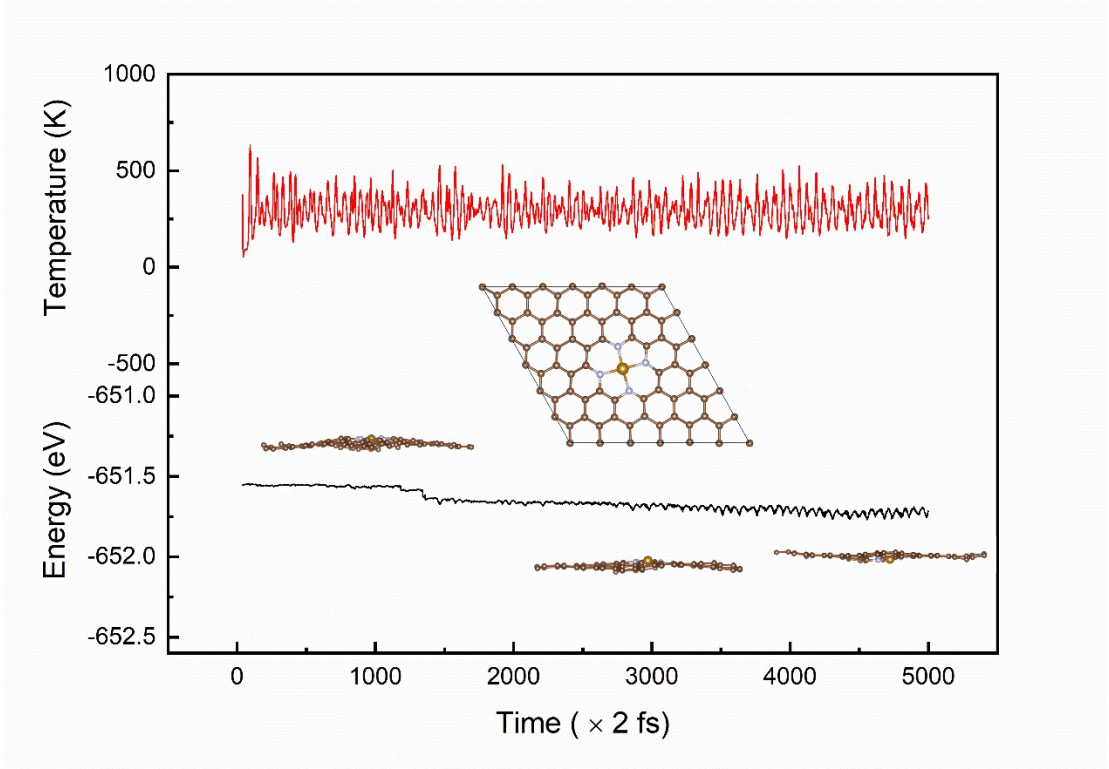

Figure S4. In the AIMD (Ab Initio Molecular Dynamics) simulation of Fe-N_4, the figure illustrates the variations in temperature and energy with respect to time. Side views of the atomic configurations at 2 ps, 6 ps, and 10 ps are shown, along with a top view at 6 ps. The simulation was carried out at 300 K over a period of 10 ps, with a time step of 2 fs.

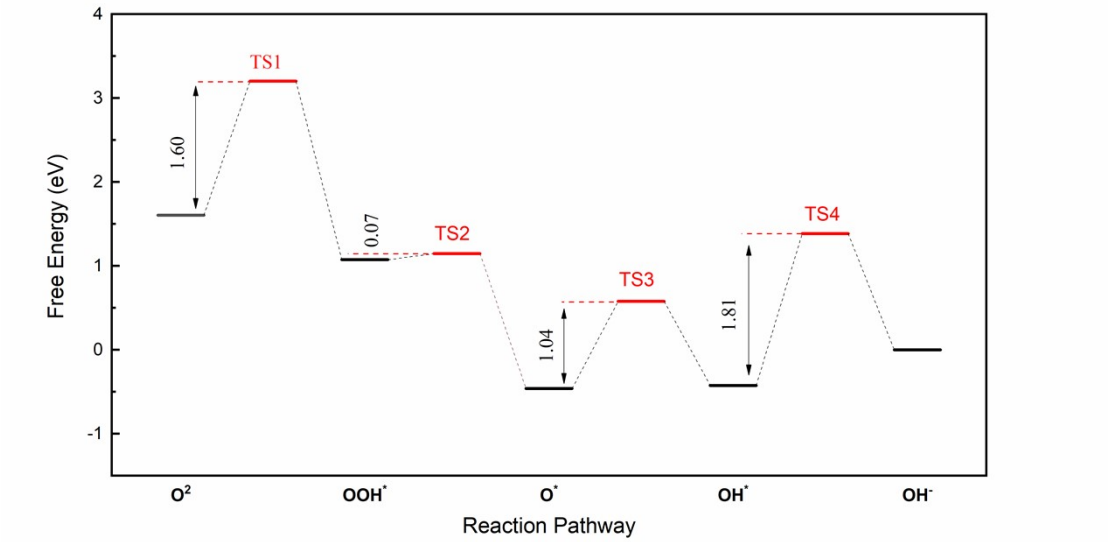

Figure S5. Transition states in the oxygen reduction reaction (ORR) pathway for the Fe-N_4 coordination structure.

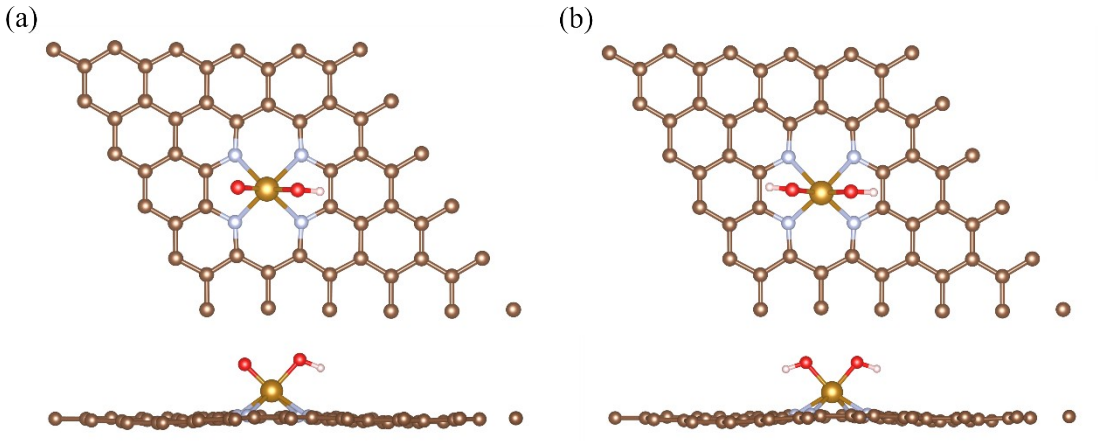

Figure S6. Coordination structure of Fe-N_4 adsorbed intermediate species (a) OH*O* and (b) OH*OH* in the structural diagrams.

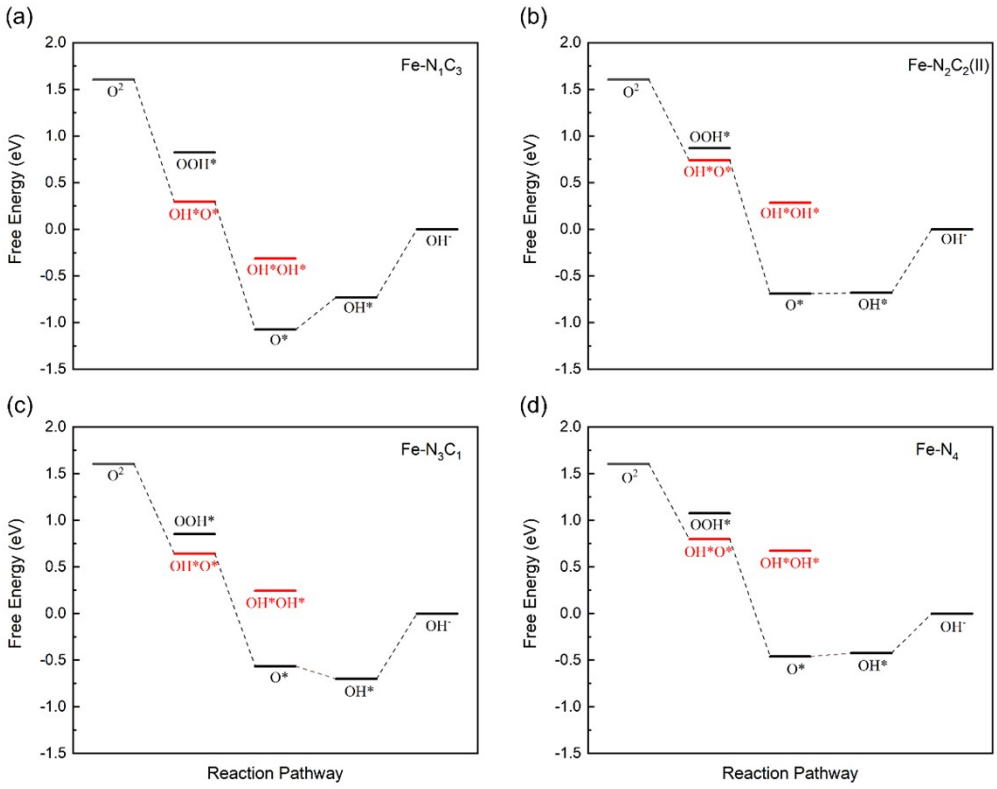

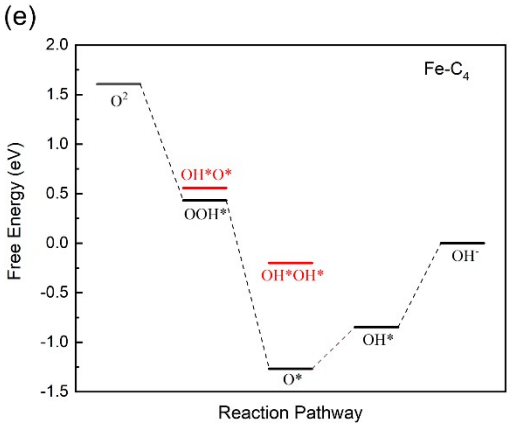

Figure S7. Gibbs energy profile of different N-coordination structures containing intermediates OH*O and OH*OH* in alkaline media at zero electrode potential (U = 0 V vs. NHE).

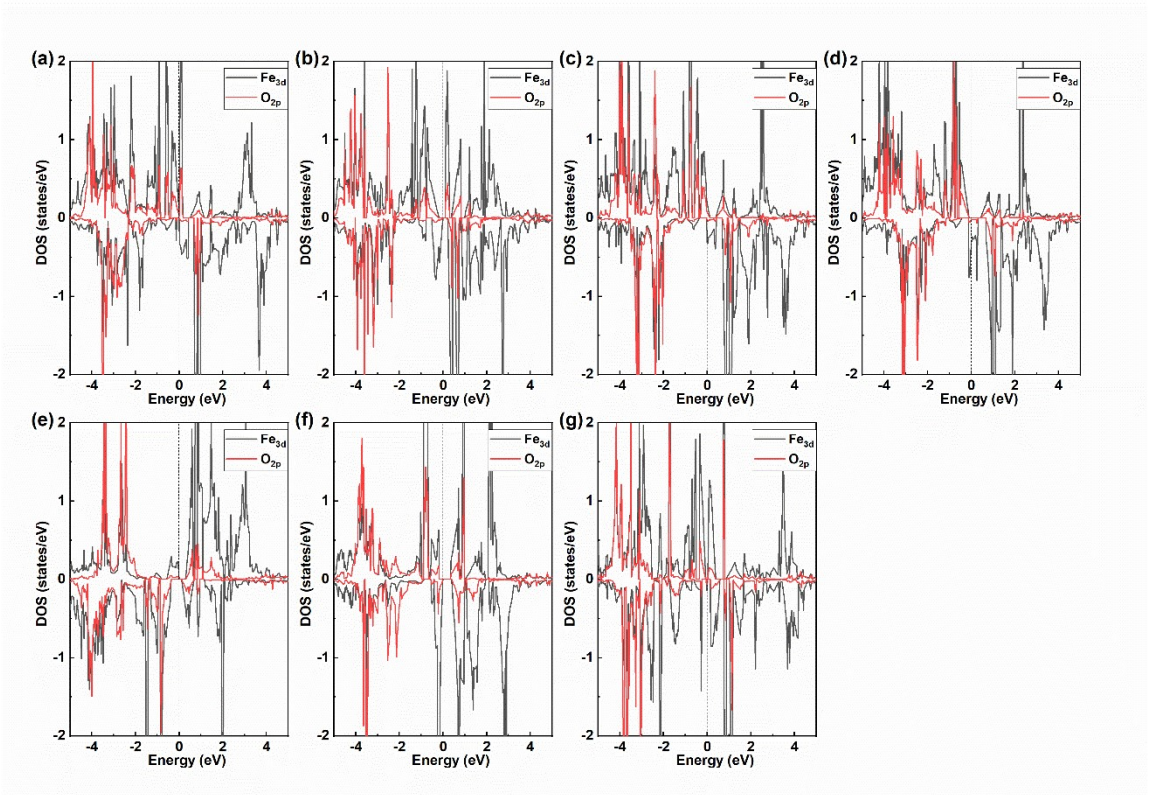

Figure S8. Projected density of states for Fe and O atoms after adsorption of *OH on different Fe-585DV/$N_xC_{(4-x)}$ structures. (a). Fe-N_1C_3, (b). Fe-N_2C_2(I), (c). Fe-N_2C2(II), (d). Fe-N_2C_2(III), (e). Fe-N_3C_1, (f). Fe-N_4. (g). Fe-C_4

Table S1 The changes in Gibbs free energy at each step of the reaction pathway (ΔG_1, ΔG_2, ΔG_3, ΔG_4) for the Gibbs energy profile in Figure S7, the Gibbs free energy of OH* adsorption (G_{OH^*}), and the overpotential (η) for different Fe-585DV/$N_xC_{(4-x)}$ structures.

Structure	ΔG_{1^*}/eV	ΔG_{2}/ev	ΔG_{3}/ev	ΔG_{4}/ev	G_{OH^*}/ev	η/ev
Fe-N_4	-0.81	-0.12	-1.10	0.42	-0.42	0.82
Fe-N_1C_3	-1.31	-0.61	-0.42	0.73	-0.73	1.13
Fe-N_2C_2(II)	-0.87	-0.46	-0.97	0.68	-0.68	1.08
Fe-N_3C_1	-0.96	-0.40	-0.94	0.70	-0.70	1.10
Fe-C_4	-1.05	-0.76	-0.65	0.85	-0.85	1.25

The ORR reaction in alkaline media at zero electrode potential (U = 0 V vs. NHE)